ADVANCED OPTICAL MATERIALS
www.advopticalmat.de

Global Photocurrent Generation in Phototransistors Based on Single-Walled Carbon Nanotubes toward Highly Sensitive Infrared Detection

Hehai Fang, Peisong Wu, Peng Wang, Zhe Zheng, Yicheng Tang, Johnny C. Ho, Gang Chen, Yueming Wang, Chongxin Shan, Xinbin Cheng, Jin Zhang,* and Weida Hu**

Because of their cost-effective synthesis and appropriate bandgap opening by various mechanisms, single-walled carbon nanotubes (SWCNTs) exhibit significant promise for highly efficient near-infrared photodetection. In this work, the first investigation of manipulating the electrode contact and exciton effect is performed on photocurrent generation of SWCNT transistors by separately depositing Cr or Pd as symmetric source/drain electrodes. Two different photoconducting behaviors of the devices, namely localized and global photocurrent generations, are then observed, where these effects are attributed to thermally assisted tunneling at the 1D-SWCNTs/3D-metal contact. A phototransistor with global photocurrent generation is demonstrated having a typical photoconductive effect with a responsivity of 2 A W^{-1} at $\lambda = 785$ nm and a fast rise (decay) time of ≈7.35 µs (11.8 µs). However, the corresponding optical response at 2000 nm is still weak due to low incident photon energy and large exciton binding energy. By further spin coating PbS quantum dots onto the SWCNTs channel, the optical response can be greatly enhanced for 2000 nm irradiation. All these results can not only illustrate the photoresponse of SWCNTs but also indicate that photogating plays a crucial role in these devices, providing valuable insights for the performance enhancement.

1. Introduction

Single-walled carbon nanotubes (SWCNTs), also known as a rolled-up regime of graphene,[1] have been widely demonstrated with distinctive electrical and optoelectronic properties because of their 1D structure and appropriate bandgap opening by manipulating their chirality and diameter.[2–8] In general, infrared photoconductivity is observed in both individual SWCNTs and SWCNTs film devices.[9,10] The ultimate goal of the scientific community is to achieve broadband CNTs-based photodetectors with remarkable performance.[11] Inevitably, when configured into photodetectors, SWCNTs still suffer from several issues for practical utilizations. First, during the device operation, the absorbed photons contribute mostly to excitons instead of free electron–hole pairs due to the large exciton binding energy of CNTs induced by

Dr. H. Fang, Dr. P. Wu, Dr. P. Wang, Dr. Y. Tang, Prof. G. Chen, Prof. Y. Wang, Prof. W. Hu
State Key Laboratory of Infrared Physics and Key Laboratory of Space Active Opto-Electronics Technology
Shanghai Institute of Technical Physics
Chinese Academy of Sciences
Shanghai 200083, China
E-mail: wdhu@mail.sitp.ac.cn

Dr. H. Fang, Dr. P. Wu, Dr. P. Wang, Prof. Y. Wang, Prof. W. Hu
University of Chinese Academy of Sciences
Beijing 100049, China

Dr. Z. Zheng, Prof. J. Zhang
Beijing Science and Engineering Center for Nanocarbons
Beijing National Laboratory for Molecular Sciences (BNLMS)
College of Chemistry and Molecular Engineering
Peking University
Beijing 100871, China
E-mail: jinzhang@pku.edu.cn

Prof. J. C. Ho
Department of Materials Science and Engineering
City University of Hong Kong
Hong Kong SAR, China

Prof. C. Shan
Henan Key Laboratory of Diamond Optoelectronic Materials and Devices
School of Physics and Engineering
Zhengzhou University
Zhengzhou 450001, China

Prof. X. Cheng
MOE Key Laboratory of Advanced Micro-Structured Materials, and Institute of Precision Optical Engineering
School of Physics Science and Engineering
Tongji University
Shanghai 200092, China
E-mail: chengxb@tongji.edu.cn

The ORCID identification number(s) for the author(s) of this article can be found under https://doi.org/10.1002/adom.201900597.

DOI: 10.1002/adom.201900597

 © 2019 WILEY-VCH Verlag GmbH & Co. KGaA, Weinheim

their 1D structure. Therefore, a relatively low electron–hole separation efficiency results. Second, although individual CNTs can have an intrinsically high mobility of up to 10^5 cm^2 V^{-1} s^{-1},[12] their thin-film counterparts composed of disordered tubes have a low mobility of even less than 10 cm^2 V^{-1} s^{-1} owing to the boundary and substrate scattering.[13] Consequently, the photogenerated carriers collected by the electrodes are limited. Third, the small-diameter CNTs with relatively large bandgaps are mostly studied for high-performance visible to near-infrared photodetection since these tubes with hybridized heterojunctions give the larger band offset and more efficient carrier migration.[14–16] However, infrared detection beyond 1550 nm achieved by SWCNTs devices is rarely reported. In this regard, tremendous efforts are devoted to extend the efficient operation of SWCNTs photodetectors to the region of longer wavelengths.

In order to achieve the broadband infrared photoresponse of CNTs devices, three main strategies are generally adopted. They are i) taking advantage of the bolometric effect by simply suspending the CNT films[17] or coupling them with other materials[11] to realize a high temperature coefficient of resistance (TCR), ii) introducing nonuniform light heating to form a temperature gradient and to drive the carrier motion within CNTs (i.e., the photo-thermoelectric effect),[18,19] and iii) enhancing the photogenerated electron–hole separation by utilizing heterostructures[14,20,21] or virtual contacts.[4] Specifically, it has been demonstrated that integrating graphdiyne with SWCNTs films can result in a nonlocal response to effectively separate the photogenerated excitons for enhanced IR detection.[2] Nevertheless, to the best of our knowledge, the impact of electrode contacts on these SWCNTs based devices has not been investigated in details until now. In the work cited herein, we fabricate SWCNTs film based phototransistors with symmetric metal contacts of Cr and Pd, respectively, to study the effect of contact electrodes on photocurrent generation and collection by scanning photocurrent mapping. It is found that Pd electrodes are more effective to collect photogenerated carriers because of the relatively small barrier for hole transport in that material. Once these SWCNT transistors are operated as a "Schottky barrier" transistor (e.g., using Cr as contact electrodes), the photocurrent is substantially degraded. In any case, using Pd symmetric contacts, the detector device delivers a fast response time as short as ≈10 µs for laser 785 nm illumination, but it still gives a deteriorated infrared response for the region of longer wavelengths. N-type PbS quantum dots are then spin-coated onto the device channel to achieve a significantly enhanced responsivity at the wavelength of 2000 nm, where this photoresponse enhancement is attributed to the photogating effect. All these results clearly indicate that photogating is an efficient approach to improve the performance of low-dimensional nanomaterials-based photodetectors.

2. Result and Discussion

Semiconducting SWCNTs used in this work were separated with the assistance of conjugated polymer (poly[9-(1-octylonoyl)-9*H*-carbazole-2,7-diyl], PCz) and deposited onto a Si/SiO_2 substrate (see the scanning electron microscope (SEM) image in Figure S1, Supporting Information). Typically,[2] 2.5 mg SWCNTs, 5.0 mg PCz, and 10.0 mL solvent (8.00 mL toluene and 2.00 mL cyclohexane) were mixed and sonicated (300 W, ≈1 h), followed by centrifuging(20 000 rpm, ≈1 h). The solution was then filtered by a polytetrafluoroethylene membrane. Subsequently, the SWCNTs left on the membrane were washed several times in toluene followed by being ultrasonicated in toluene for 10 min and centrifuged (40 000 rpm). Repeating these steps will remove most of the PCz wrapped on the SWCNTs. Raman spectrum of the as-prepared SWCNTs film is presented in **Figure 1**a. It is clear that the *G*-band feature consists of two high-contrast components with one peak at 1570 cm^{-1} (*G*–) and another peak at 1592 cm^{-1} (G^+), which indicate the good semiconducting property of the tubes instead of the metallic one.[22] The solution absorption spectra further confirm the high purity of semiconducting SWCNTs (see Figure S2 in the Supporting Information).

In order to verify the electrical property of the obtained SWCNTs film, we first fabricated thin-film field-effect transistors using Cr/Au (15/45 nm) as the symmetric and interdigital electrodes by thermal evaporation (Figure S1, Supporting Information). As depicted in the device transfer characteristic (I_{ds}–V_g curve) measured at V_{ds} = 1 V, the device shows a hole-dominated transport behavior, while the majority carrier can also be tuned to be the electron if a sufficiently large positive gate voltage is applied (Figure 1b). Moreover, the on/off current ratio exceeds 10^6, whereas the off current can be manipulated to be as low as 10^{-11} A, further confirming the high purity of the semiconducting SWCNTs. Notably, when the device output is measured in the dark and under the halogen lamp illumination, the I_{ds}–V_g curves remain the same, which indicates no significant photocurrent generation. This conclusion is also confirmed with the measurement of the output characteristic (I_{ds}–V_{ds} curve) performed in the dark and under the illumination (data not shown); again, there is no evident photocurrent observed.

To investigate the reason behind this result, scanning photocurrent mappings were conducted. In details, a chopped near-infrared laser (λ = 785 nm, f = 933 Hz) was focused onto the device channel surface through a 20× objective lens. The laser spot (with a diameter of ≈3 µm) could then be scanned in a 2D plane to excite the local photocurrent, which was subsequently recorded by a lock-in phase amplifier. According to the mapping results (measured at V_{ds} = 0.1 V) as displayed in Figure 1c, the photocurrent generation appears in proximity to the electrodes, while the photocurrent generation directions at source and drain regions are opposite to each other. To identify the photocurrent distribution, a photocurrent slice perpendicular to the cross fingers is given in Figure 1d. Although the extracted photocurrent fluctuates slightly due to the background noise, it is evident that the peak and valley values are located at the electrode edges. In addition, the shape of each peak or valley is almost symmetric such that four Gaussian functions can then be applied to fit the curve (Figure 1d). The corresponding full width at half maximum (FWHMs) of all peaks are ≈3 µm, which is equal to the light spot size. This result demonstrates that the photocurrent is only generated at the electrode/SWCNT contacting edge, justifying the existence of the very weak global photocurrent as discussed above. Additional photocurrent mappings were also conducted at lager bias voltages such as 0.5 and 1 V. However, the collected signal is completely buried

© 2019 WILEY-VCH Verlag GmbH & Co. KGaA, Weinheim

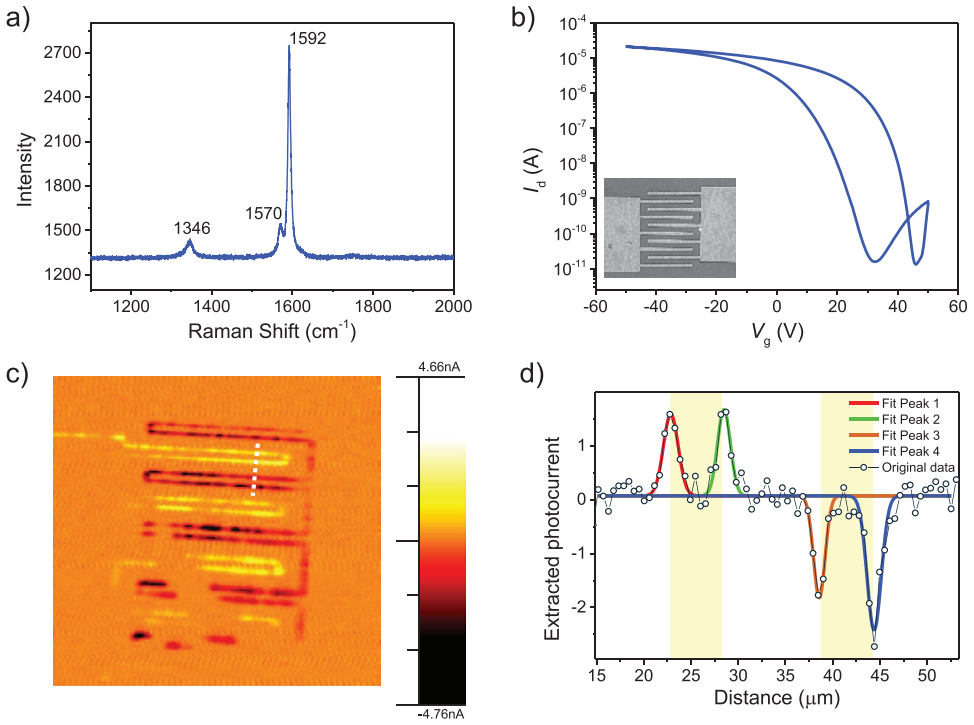

Figure 1. SWCNT field effect transistors using Cr/Au as source/drain electrodes. a) Raman spectra of the as-prepared SWCNT film. b) Transfer characteristics of the fabricated FET. Inset is the SEM image of the device. c) Photocurrent mapping. d) Photocurrent slice perpendicular to the cross fingers as denoted by the white dashed line in c). The shallow-yellow regions indicate the electrodes.

within the noise current. Such a local response has also been observed in our previous work, where it is mainly attributed to the large binding energy of electron–hole pairs that contribute to the excitons.[2] Nevertheless, there is very limited study on the impact of electrode metal on the photocurrent generation even though the photovoltaic effect or the photo-thermoelectric effect is observed to lead to a similar local response.[18,23]

In the succeeding experiments, Pd/Au (15/45 nm) instead of Cr/Au was deposited as the source/drain electrodes for device fabrication. Pd is a metal with a relatively high work function (5.12 eV), which is favorable for p-type semiconductors in the formation of Ohmic contact. Photocurrent mapping was also conducted on those devices with the result presented in **Figure 2**a (V_{ds} = 0.1 V). It is clear that significant photocurrents have been generated from the SWCNT channels, in which the generation is no longer restricted to the electrode/SWCNT contacting edges. This observation is totally different from that of the device using Cr/Au electrodes. Figure 2b depicts the photoresponse speed of the device measured at V_{ds} = 5 V, λ = 785 nm, P = 350 μW, without applying any gate voltage. The rise time and decay time are found to be 7.35 and 11.8 μs, respectively, which are relatively fast among CNTs film based detectors.[2,4,15,24–28] Furthermore, the dependence of the net photocurrent on the bias voltage exhibits a linear relationship, indicating a typical photoconductive effect (Figure 2c). As shown in Figure 2d, the responsivities are carefully measured at various gate voltages for incident wavelengths of 785 and 2000 nm, respectively (V_{ds} = 1 V, P = 58 μW). It is clearly observed that the responsivity increases with a more negative gate voltage, while the response at 2000 nm is much weaker than that at 785 nm. Specifically, the responsivity approaches ≈2 A W^{-1} when V_g is −16 V and irradiation wavelength is 785 nm, but decreases to less than 10^{-4}A W^{-1} at V_g = 8 V for both irradiation wavelengths of 785 and 2000 nm (see more details and discussions in Figures S3 and S4 in the Supporting Information). This inadequate performance would not be sufficient for practical near-IR photodetection.

It is worth mentioning that when electrodes of Pd/Au are utilized instead of Cr/Au for device fabrication, the weak and localized photoresponse is changed to an evident and global one, illustrating the substantial impact of metal contacts on the optoelectronic performance of SWCNT based devices. Early in 2002, it was demonstrated that the CNT device can operate as a "Schottky barrier" transistor,[29] where the transistor behavior is mainly dominated by varying the contact resistance rather than the channel conductance. Because of the 1D characteristic of SWCNTs, thermally assisted tunneling plays a crucial role in regulating their electrical and optoelectronic properties, especially when the Fermi level of the metal approaches the middle of the bandgap of CNTs.[29,30] For the case of Cr, which has a work function of ≈4.6 eV, it is near to the bandgap center of SWCNTs (≈3.8–5.2 eV). In this case, once Cr is deposited as the electrode contact, the hole-injection phenomenon becomes a tunneling process(**Figure 3**a). The tunneling current is then determined by the barrier height and width, of which the latter can be modulated by both the gate voltage and bias voltage. Because of the relatively large contact barrier, the applied bias voltage primarily drops at the contact region, while the actual bias applied on the SWCNTs channel is very small, leading to an almost flat band condition (Figure 3a). Under illumination,

© 2019 WILEY-VCH Verlag GmbH & Co. KGaA, Weinheim

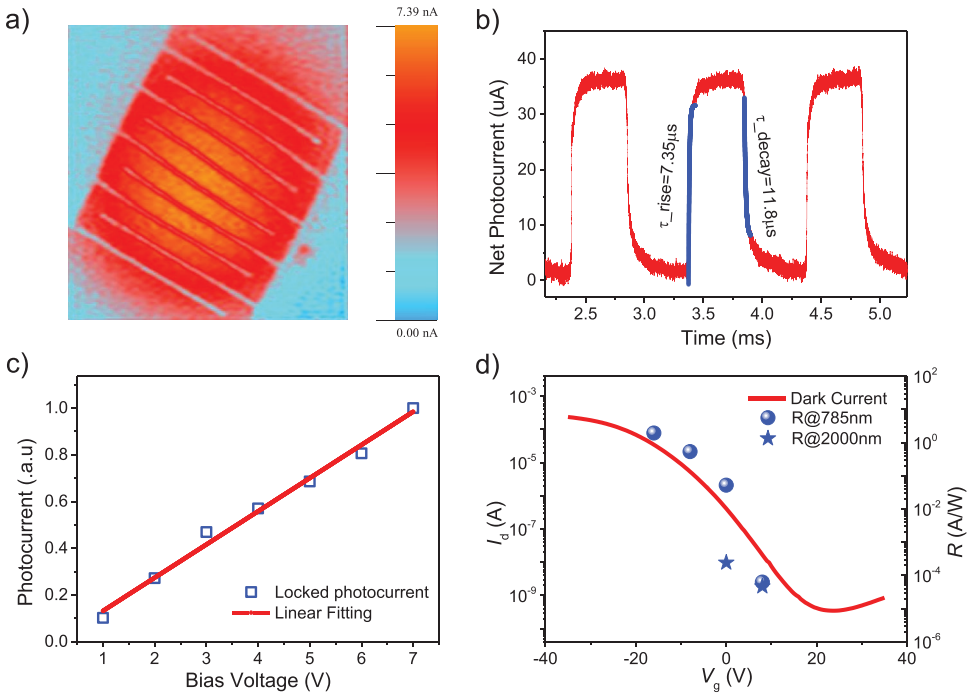

Figure 2. Optoelectronic characterizations of SWCNTs field-effect transistors using Pd/Au as electrodes. a) Photocurrent mapping conducted at $V_{ds} = 0.1$ V, $\lambda = 785$ nm. b) Temporal photoresponse. c) Photocurrent dependence on the bias voltage. d) Responsivities for incident light of 785 and 2000 nm, measured at various gate voltages.

the photocarriers generated from the SWCNTs would move to the electrodes under the very small electric field. However, since there is a lack of the significant external electric field, the exciton effect in the 1D SWCNTs would exist. In other words, the photoexcited electron–hole pairs in the SWCNTs channel are not efficiently separated, and thus hardly contributing to the photocurrent. As a result, the observed local photocurrent restricted around the electrode edges is probably due to the photovoltaic effect induced by the built-in field formed at the metal/semiconductor contacting interface. For a larger applied bias voltage, the barrier width is modulated accordingly, but the actual bias applied on the SWCNTs channel changes insignificantly because of the property of "Schottky barrier" transistors (Figure 3b). In this way, the dark current increases, while the signal-to-noise ratio decreases correspondingly. On the other hand, when Pd (work function of ≈5.12 eV) is used as the electrode contact, the SWCNTs would operate as a p-type semiconductor since the Fermi level of Pd is close to the valance band of SWCNTs. In this case, the Schottky barrier for holes becomes relatively small so that the device can function as a normal

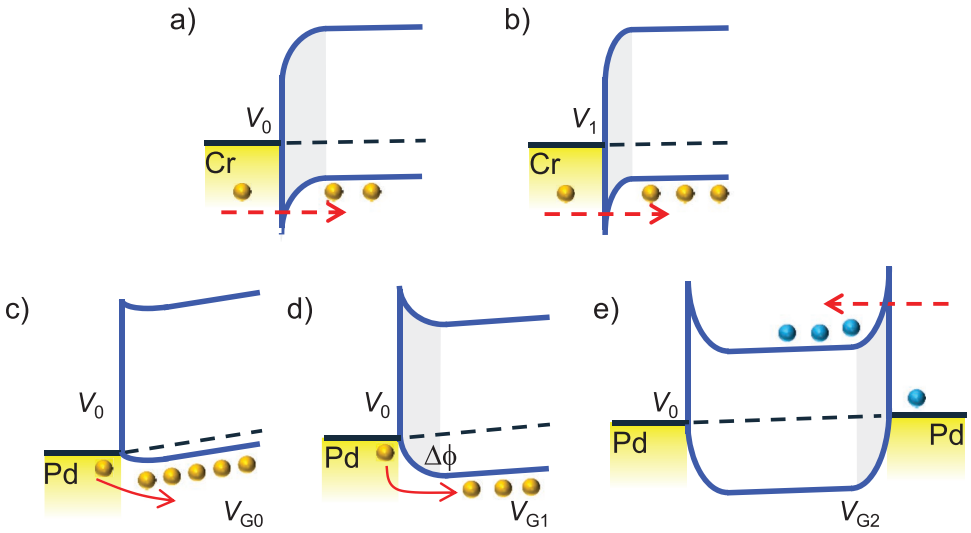

Figure 3. Schematic energy band diagrams when using a,b) Cr, c-e) Pd as the electrode contacts. Bias voltage $V_1 > V_0$, gate voltage $V_{G2} > V_{G1} > V_{G0}$.

© 2019 WILEY-VCH Verlag GmbH & Co. KGaA, Weinheim

field-effect transistor instead of a "Schottky barrier" transistor.[29] In this case, the applied voltage is observed to mainly drop across the SWCNTs channel, whereas the photocarriers would yield a significant photocurrent that can be measured (Figure 3c). When the gate voltage tunes the Fermi level of electrode away from the valance band of the device channel, the hole concentration decreases consequently and the hole injection by thermal emission is gradually blocked by the increased barrier height (Figure 3d). Therefore, the actual voltage applied on the SWCNTs channel becomes smaller, and hence the photocurrent decays. For a larger applied positive gate voltage, the electron injection would be activated at the other metal contact due to the tunneling induced by the reduced barrier width (Figure 3e). As a result, the SWCNTs transistor is operated as a "Schottky barrier" transistor again, wherein the global photocurrent becomes zero.

After this analysis and discussion, it is seen that the previously reported hybrid SWCNTs/graphdiyne device can efficiently improve its photoresponse even when using Cr/Au as the contact electrodes.[2] In this hybrid device structure, the exciton effect has been greatly suppressed because of the built-in electric field that existed at the interface of between SWCNTs and graphdiyne; thus, a nonlocal photoresponse resulted. In contrast, for our SWCNT transistors using Pd as the contacts, the exciton effect may not necessarily be the biggest hurdle that hinders the device photoresponse. As confirmed by the photocurrent mapping result presented in Figure 2a, the exciton effect can be effectively overcome by the external electric field established in our devices, indicating the potential of our simple device structure for highly efficient near-IR photodetection.

Aside from the above-discussed issue of contact resistance, more performance parameters of our SWCNTs devices can be further evaluated. Specifically, based on the linear region of transfer characteristics of the SWCNTs transistor, a hole mobility (μ) of ≈10 $cm^2\ V^{-1}\ s^{-1}$ is estimated (Figure 2d). For V_{ds} = 1 V and irradiation wavelength of 785 nm, the device responsivity is found to be 2 A W^{-1}. The corresponding photogain is ≈40, which can be estimated from the relationship of $R = G \times \eta \times \lambda q/hc$ (G is the photoconductive gain, and η is the optical absorption with the value of ≈8% here). The gain can also be derived by the ratio of between carrier lifetime and transit time, as denoted by $G = \tau/(L^2/\mu V_{ds})$, where τ is the carrier lifetime, and L is the device channel length. As a consequence, a lifetime of ≈16 µs is deduced. The estimated lifetime is in a good agreement with the measured response time (Figure 2b); however, this contributes to unusually long lifetime values since the carrier lifetime of the first excited state of SWCNTs is typically found to be on the order of picoseconds.[31–33] In 2004, Wang et al.[34] reported an indirectly measured radiative carrier lifetime of SWCNTs as long as ≈110 ns. Also, the tight-binding model of quasi-1D systems gave a theoretical room-temperature lifetime of 180–240 ns for SWCNTs.[34] To the best of our knowledge, there is no reported lifetime of SWCNTs as long as tens of microseconds which was observed in our work. Such a long carrier lifetime of our SWCNTs photodetectors can be attributed to unintentional impurities introduced during the solution-processed purification and subsequent device fabrication, which bring together the trap states and hence prolong the carrier lifetime.

Although the exciton effect can be overcome by the applied electric field when using Pd as the electrodes, there is still an issue to employ these SWCNTs devices for the photodetection of infrared photons with lower energies. It is evident that the optical absorption of SWCNTs at 2000 nm is quite comparable to that at 785 nm (see Figure S2 in the Supporting Information), but the responsivity at 2000 nm is much lower there (Figure 2d). In order to boost the infrared response of our devices, n-type PbS quantum dots (QDs)[35] were spin coated onto the fabricated SWCNT transistors. Previously reported work[20,24] has adopted a similar method to enhance the responsivity of SWCNT transistors. However, the detection wave range is mostly determined by the optical absorption of QDs and the infrared photoresponse contributed by the intrinsic S_{11} absorption of SWCNTs (≈1600–2000 nm, see Figure S2 in the Supporting Information) has always been ignored. Here the built-in electric field existed between SWCNTs and QDs is expected to promote the electron–hole separation and enhance the infrared photoresponse even at 2000 nm. At first, we investigated the photocurrent generation in this hybrid structure. As shown in the photocurrent mapping at λ = 785 nm (**Figure 4**a), there is an evident photocurrent generated from the device channel. Unlike the angular mapping shape of devices without QDs (Figure 2a), the square corners of this current mapping are bent and the edges become distorted. This phenomenon is probably due to the fact that the photoexcited carriers generated nearby QDs are also transferred to the SWCNTs channel, and hence contribute to the photocurrent.[24] We then measured the responsivities at various incident powers of 785 nm laser (Figure 4b), where a typical power law of $R \propto P^{-0.65}$ is obtained. At low incident powers of less than 0.05 µW, the responsivity approaches 10 A W^{-1}; however, the temporal response speed becomes much slower than before without any QD deposition (Figure 4c). It takes an acceptable τ_{rise} of ≈90 ms followed by a slow τ_{rise2} of more than 10 s for the photocurrent to be stable under illumination. The decay times are more or less the same. As a result, the responsivity is improved at the cost of response speed, which is commonly observed for photoresponse dominated by defects or trap states induced photogating.[36–39] A better interface quality of between SWCNTs and QDs by precisely controlling the spin-coating parameters and regulating the unintentional impurities during spin coating would lead to the faster response. At the same time, the optical responses at different chopping frequencies of the incident light were also measured as shown in Figure 4d. The photocurrent is found to decay quickly with the increasing chopping frequency, but it can still be clearly observed even for a frequency higher than 1 kHz because of the minority carriers with the shorter lifetimes.

Moreover, the device transfer characteristics were measured in the dark and under laser illuminations at 785, 1550, and 2000 nm, respectively, with the same incident power of 58 µW as shown in **Figure 5**a. The comparison of transfer curves before and after spinning-coating of QDs is presented in Figure S5 in the Supporting Information. It is clear that the typical photogating behavior is observed for the device (Figure 5a, inset), wherein the device threshold voltage is shifted toward the positive direction under all different illuminations. The photoresponse at 2000 nm is the weakest among the different three wavelengths, because both SWCNTs and

© 2019 WILEY-VCH Verlag GmbH & Co. KGaA, Weinheim

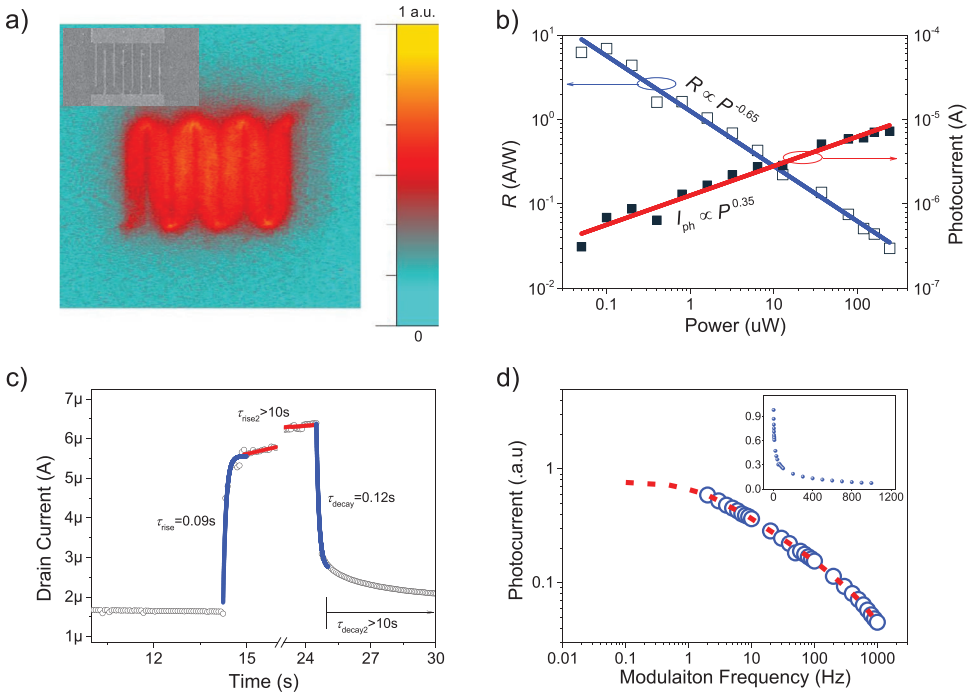

Figure 4. Optoelectronic characterizations at $\lambda = 785$ nm on the hybrid SWCNTs/QDs detector. a) Photocurrent mapping at $V_{ds} = 1$ V without applying gate voltage. b) Responsivity and photocurrent dependence on incident light power. c) Rise and decay behaviors of the photocurrent. d) Photocurrent dependence on the light modulation frequency.

QDs can absorb the photons of 785 and 1550 nm while only SWCNTs can absorb those at 2000 nm. The optical absorption details can be referred to the normalized absorption spectrums of QDs and SWCNTs as depicted in Figure 5c (inset). Additional device output characteristics were then measured in the dark and under the illumination of 2000 nm laser with various powers (Figure 5b). Similar to most of photoconductors, a higher applied bias voltage and stronger incident light power would lead to the larger net photocurrent. It is noted that because of the photogating effect, the dependence of net photocurrent on the bias voltage and light power obeys the following relationship of $I_{ph} \propto V_{ds} \times P^{\alpha}$, where $0 < \alpha < 1$.[36] This nonlinear dependence of responsivity on the incident light power would guarantee high sensitivity in weak light conditions. In addition, the response spectrum (700–1800 nm) of the fabricated hybrid SWCNTs/QDs phototransistor was also measured at $V_{ds} = 1$ V and $P = 10$ µW without applying any gate voltage (Figure 5c). There are two response peaks observed at around 1100 and 1450 nm, which are attributed to the peak absorption of SWCNTs and QDs, respectively. At the same bias and power condition for the irradiation wavelength of 2000 nm, the device responsivity of 39 mA W^{-1} is obtained, and is also plotted against the response spectrum (see more details about the spectrum measurement in Figure S6 in the Supporting Information). Obviously, this hybrid device exhibits a greatly enhanced infrared photoresponse as compared to the pure SWCNTs phototransistor (<1 mA W^{-1} at 2000 nm, Figure 2d).

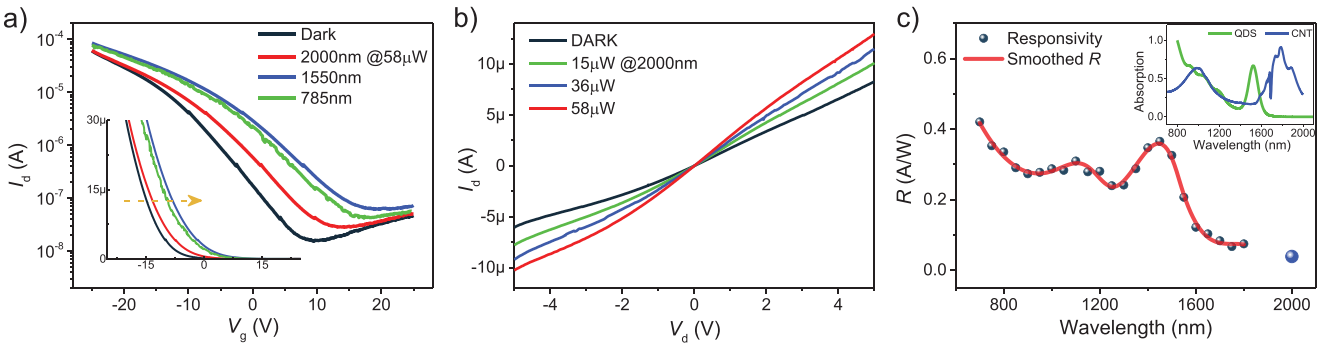

Figure 5. Infrared photoresponse of the hybrid SWCNTs/QDs phototransistor. a) I_{ds}–V_g transfer characteristics ($V_{ds} = 1$ V) in the dark and under the illuminations of different wavelengths with the same incident light power. Inset is the linear plot. b) I_{ds}–V_{ds} curves in the dark and under the illuminations of 2000 nm light at various incident light powers, without applying any gate voltage. c) Photoresponse spectrum measured at $V_{ds} = 1$ V, $P = 10$ µW, without applying any gate voltage.

© 2019 WILEY-VCH Verlag GmbH & Co. KGaA, Weinheim

3. Conclusion

In conclusion, we performed a comprehensive investigation of the impacts of electrode contacts on the optical response of SWCNTs phototransistors by using Cr and Pd as the symmetric contacts. When Cr is utilized, the device exhibits a local photoresponse restricted to the area around the source/drain electrodes with opposite current direction. Once Pd is used, the phototransistor shows significant photoresponse originating from the SWCNTs channel, especially when a more negative gate voltage is applied to switch the device into the p-type state. Since the current injection is dominated by the thermally assisted tunneling, the devices would not show any photoresponse when they operate as "Schottky barrier" transistors. Furthermore, the pure SWCNTs phototransistors, using Pd as the symmetric contacts, deliver a respectable responsivity of 2 A W^{-1} for the irradiation wavelength of 785 nm as well as a fast rise (decay) time of ≈7.35 µs (11.8 µs). The exciton effect may not necessarily be the biggest obstacle that hinders the device optical response, but it would become crucial for the photodetection of infrared photons with lower energies. By spin coating PbS quantum dots onto the SWCNTs channel, a built-in electric field at the nanotube/QD interface is established for the photogating effect and results in the enhanced photoresponsivity at the wavelength of 2000 nm. All these results can provide a valuable insight into the design and fabrication of high-performance infrared photodetectors based on SWCNTs.

Supporting Information

Supporting Information is available from the Wiley Online Library or from the author.

Acknowledgements

H.H.F. and P.S.W. contributed equally to this work. This work was supported by the National Natural Science Foundation of China (Grant Nos. 61725505, 11734016, and 61521005), Key research project of frontier science of Chinese Academy of Sciences (CAS) (Grant No. QYZDB-SSW-JSC031), Program of Shanghai Subject Chief Scientist (Grant No.19XD1404100), Natural Science Foundation of Shanghai (Grant Nos. 18ZR1445800, 18ZR1445900, and 19YF1454600), Yao Foundation (CX-140), and Fund of SITP Innovation Team (CX-239). The authors thank James Torley from the University of Colorado at Colorado Springs for critical reading of the manuscript.

Conflict of Interest

The authors declare no conflict of interest.

Keywords

infrared photodetectors, PbS quantum dots, photogating, phototransistors, singe-walled carbon nanotubes

Received: April 10, 2019
Revised: August 3, 2019
Published online:

[1] A. K. Geim, K. S. Novoselov, *Nat. Mater.* **2007**, *6*, 183.
[2] Z. Zheng, H. H. Fang, D. Liu, Z. J. Tan, X. Gao, W. D. Hu, H. L. Peng, L. M. Tong, W. P. Hu, J. Zhang, *Adv. Sci.* **2017**, *4*, 1700472.
[3] R. S. Park, M. M. Shulaker, G. Hills, L. S. Liyanage, S. Lee, A. Tang, S. Mitra, H. S. Wong, *ACS Nano* **2016**, *10*, 4599.
[4] Y. Liu, N. Wei, Q. Zeng, J. Han, H. Huang, D. Zhong, F. Wang, L. Ding, J. Xia, H. Xu, Z. Ma, S. Qiu, Q. Li, X. Liang, Z. Zhang, S. Wang, L.-M. Peng, *Adv. Opt. Mater.* **2016**, *4*, 238.
[5] F. Hennrich, W. Li, R. Fischer, S. Lebedkin, R. Krupke, M. M. Kappes, *ACS Nano* **2016**, *10*, 1888.
[6] Y. M. Chen, X. Y. Yu, Z. Li, U. Paik, X. W. Lou, *Sci. Adv.* **2016**, *2*, e1600021.
[7] H. P. Komsa, R. Senga, K. Suenaga, A. V. Krasheninnikov, *Nano Lett.* **2017**, *17*, 3694.
[8] K. S. Burch, *Nat. Nanotechnol.* **2018**, *13*, 532.
[9] M. Freitag, Y. Martin, J. A. Misewich, R. Martel, P. H. Avouris, *Nano Lett.* **2003**, *3*, 1067.
[10] I. A. Levitsky, W. B. Euler, *Appl. Phys. Lett.* **2003**, *83*, 1857.
[11] X. He, F. Léonard, J. Kono, *Adv. Opt. Mater.* **2015**, *3*, 989.
[12] T. Durkop, S. A. Getty, E. Cobas, M. S. Fuhrer, *Nano Lett.* **2004**, *4*, 35.
[13] C. Cao, J. B. Andrews, A. Kumar, A. D. Franklin, *ACS Nano* **2016**, *10*, 5221.
[14] R. Lu, C. Christianson, A. Kirkeminde, S. Ren, J. Wu, *Nano Lett.* **2012**, *12*, 6244.
[15] S. Park, S. J. Kim, J. H. Nam, G. Pitner, T. H. Lee, A. L. Ayzner, H. Wang, S. W. Fong, M. Vosgueritchian, Y. J. Park, M. L. Brongersma, Z. Bao, *Adv. Mater.* **2015**, *27*, 759.
[16] D. J. Bindl, M. Y. Wu, F. C. Prehn, M. S. Arnold, *Nano Lett.* **2011**, *11*, 455.
[17] M. E. Itkis, F. Borondics, A. Yu, R. C. Haddon, *Science* **2006**, *312*, 413.
[18] S. Nanot, A. W. Cummings, C. L. Pint, A. Ikeuchi, T. Akiho, K. Sueoka, R. H. Hauge, F. Leonard, J. Kono, *Sci. Rep.* **2013**, *3*, 1335.
[19] X. W. He, X. Wang, S. Nanot, K. Cong, Q. J. Jiang, A. A. Kane, J. E. M. Goldsmith, R. H. Hauge, F. Leonard, J. Kono, *ACS Nano* **2013**, *7*, 7271.
[20] D. Wang, J. K. Baral, H. Zhao, B. A. Gonfa, V.-V. Truong, M. A. El Khakani, R. Izquierdo, D. Ma, *Adv. Funct. Mater.* **2011**, *21*, 4010.
[21] Y. Liu, F. Wang, X. Wang, X. Wang, E. Flahaut, X. Liu, Y. Li, X. Wang, Y. Xu, Y. Shi, R. Zhang, *Nat. Commun.* **2015**, *6*, 8589.
[22] M. S. Dresselhaus, G. Dresselhaus, R. Saito, A. Jorio, *Phys. Rep.* **2005**, *409*, 47.
[23] B. C. St-Antoine, D. Ménard, R. Martel, *Nano Res.* **2012**, *5*, 73.
[24] Y. C. Tang, H. H. Fang, M. S. Long, G. Chen, Z. Zheng, J. Zhang, W. J. Zhou, Z. J. Ning, Z. H. Zhu, Y. Feng, S. G. Qin, X. S. Chen, W. Lu, W. D. Hu, *IEEE J. Sel. Top. Quantum Electron.* **2018**, *24*, 1.
[25] T. F. Zhang, Z. P. Li, J. Z. Wang, W. Y. Kong, G. A. Wu, Y. Z. Zheng, Y. W. Zhao, E. X. Yao, N. X. Zhuang, L. B. Luo, *Sci. Rep.* **2016**, *6*, 38569.
[26] G. Li, M. Suja, M. Chen, E. Bekyarova, R. C. Haddon, J. Liu, M. E. Itkis, *ACS Appl. Mater. Interfaces* **2017**, *9*, 37094.
[27] Y. Liu, Y. Liu, S. Qin, Y. Xu, R. Zhang, F. Wang, *Nano Res.* **2017**, *10*, 1880.
[28] S. Liang, Z. Ma, G. Wu, N. Wei, L. Huang, H. Huang, H. Liu, S. Wang, L. M. Peng, *ACS Nano* **2016**, *10*, 6963.
[29] S. Heinze, J. Tersoff, R. Martel, V. Derycke, J. Appenzeller, P. Avouris, *Phys. Rev. Lett.* **2002**, *89*, 106801.
[30] J. Appenzeller, M. Radosavljevic, J. Knoch, P. Avouris, *Phys. Rev. Lett.* **2004**, *92*, 048301.
[31] T. Hertel, G. Moos, *Phys. Rev. Lett.* **2000**, *84*, 5002.
[32] T. Hertel, R. Fasel, G. Moos, *Appl. Phys. A: Mater. Sci. Process.* **2002**, *75*, 449.

 © 2019 WILEY-VCH Verlag GmbH & Co. KGaA, Weinheim

[33] S. Reich, M. Dworzak, A. Hoffmann, C. Thomsen, M. S. Strano, *Phys. Rev. B* **2005**, 71.
[34] F. Wang, G. Dukovic, L. E. Brus, T. F. Heinz, *Phys. Rev. Lett.* **2004**, *92*, 177401.
[35] Z. Ning, O. Voznyy, J. Pan, S. Hoogland, V. Adinolfi, J. Xu, M. Li, A. R. Kirmani, J. P. Sun, J. Minor, K. W. Kemp, H. Dong, L. Rollny, A. Labelle, G. Carey, B. Sutherland, I. Hill, A. Amassian, H. Liu, J. Tang, O. M. Bakr, E. H. Sargent, *Nat. Mater.* **2014**, *13*, 822.
[36] H. H. Fang, W. D. Hu, *Adv. Sci.* **2017**, *4*, 1700323.
[37] S. Goossens, G. Navickaite, C. Monasterio, S. Gupta, J. J. Piqueras, R. Pérez, G. Burwell, I. Nikitskiy, T. Lasanta, T. Galán, E. Puma, A. Centeno, A. Pesquera, A. Zurutuza, G. Konstantatos, F. Koppens, *Nat. Photonics* **2017**, *11*, 366.
[38] C. Hu, D. Dong, X. Yang, K. Qiao, D. Yang, H. Deng, S. Yuan, J. Khan, Y. Lan, H. Song, J. Tang, *Adv. Funct. Mater.* **2017**, *27*, 1603605.
[39] N. Guo, F. Gong, J. K. Liu, Y. Jia, S. F. Zhao, L. Liao, M. Su, Z. Y. Fan, X. S. Chen, W. Lu, L. Xiao, W. D. Hu, *ACS Appl. Mater. Interfaces* **2017**, *9*, 34489.

© 2019 WILEY-VCH Verlag GmbH & Co. KGaA, Weinheim